Proc. Natl. Acad. Sci. USA
Vol. 87, pp. 5715–5719, August 1990
Physiology/Pharmacology

Ion microscopic imaging of calcium transport in the intestinal tissue of vitamin D-deficient and vitamin D-replete chickens: A ^{44}Ca stable isotope study

SUBHASH CHANDRA*, CURTIS S. FULLMER†, CHRISTINA A. SMITH‡, ROBERT H. WASSERMAN†, AND GEORGE H. MORRISON*

Departments of *Chemistry, †Veterinary Physiology, and ‡Veterinary Pathology, Cornell University, Ithaca, NY 14853

Contributed by Robert H. Wasserman, May 4, 1990

ABSTRACT **The intestinal absorption of calcium includes at least three definable steps: transfer across the microvillar membrane, movement through the cytosolic compartment, and energy-dependent extrusion into the lamina propria. Tracing the movement of calcium through the epithelium has been hampered by lack of suitable techniques and, in this study, advantage was taken of ion microscopy in conjunction with cryosectioning and use of the stable isotope ^{44}Ca to visualize calcium in transit during the absorptive process. The effect of vitamin D, required for optimal calcium absorption, was investigated. Twenty millimolar ^{44}Ca was injected into the duodenal lumen *in situ* of vitamin D-deficient and vitamin D-replete chickens. At 2.5, 5.0, and 20.0 min after injection, duodenal tissue was obtained and processed for ion microscopic imaging. At 2.5 min, ^{44}Ca was seen to be concentrated in the region subjacent to the microvillar membrane in tissue from both groups. At 5.0 and 20.0 min, a similar pattern of localization was evident in D-deficient tissues. In D-replete tissues, the distribution of ^{44}Ca became more homogenous, indicating that vitamin D increased the rate of transfer of Ca^{2+} from the apical to the basolateral membrane, a function previously ascribed to the vitamin D-induced calcium-binding protein (28-kDa calbindin-D). Quantitative aspects of the calcium absorptive process were determined in parallel experiments with the radionuclide ^{47}Ca. Complementary information on the localization of the naturally occurring isotopes of calcium (^{40}Ca) and potassium (^{39}K) is also described.**

The past 20 years have been marked by a growing recognition of the important role of calcium (Ca) as a second messenger, involved in the mediation of a diverse array of cellular functions (1). As a major component of bones and teeth, large amounts of Ca are required for their formation. The only source of Ca to meet these essential functions is ultimately the diet, and mechanisms have evolved to assure an adequate and proper transfer of dietary Ca across the intestine. Special accommodations must be made by the intestinal epithelial cells to transport the large quantities of Ca and, at the same time, assure that the intracellular free Ca^{2+} concentrations are maintained at levels that are nontoxic and appropriate for normal cell function.

A complete understanding of the Ca absorption process and the role of vitamin D thereon, despite considerable effort, is still lacking. One aspect that requires clarification is the path taken by Ca during its transport across epithelia. In the present study, we have visualized this transport by using the stable isotope ^{44}Ca as the absorbed species in combination with the technique of ion microscopy (2–4). The ion microscope, based on secondary ion mass spectrometry, is a direct imaging mass spectrometer. The instrument can discriminate isotopes based on their mass-to-charge ratio and, therefore, allows imaging of isotopic gradients in relation to tissue morphology with a spatial resolution of ≈ 0.5 μm. Because the analysis is made by sputtering the sample surface in the Z direction, the distribution of several isotopes can be imaged from the same specimen. This specific capability of the ion microscope has allowed visualization of ^{44}Ca during its absorption and, at the same time, localization of the naturally occurring major isotope of calcium, ^{40}Ca. In an attempt to further understand the process of intestinal Ca transport and the stimulatory role of vitamin D on this process, we have visually compared the transport of luminally administered ^{44}Ca in vitamin D-deficient and vitamin D-replete chickens.

MATERIALS AND METHODS

Hatchling White Leghorn cockerels (Clock and De Cloux, Ithaca, NY) were fed a semisynthetic vitamin D-deficient diet (5) for 4 weeks. Seventy-two hours before experiment, one half of the chickens were dosed (i.m.) with 500 international units of vitamin D_3 in propylene glycol (vitamin D-replete chickens). All chickens were fasted from food, but not water, for 16 hr immediately before the experiment. The *in situ*-ligated duodenal loop procedure (6) was used for both ion microscopic and radioactive ^{47}Ca absorption studies. For visualizing calcium by ion microscopy, 1 ml of a solution containing 20 mM $^{44}CaCl_2$ (98.78% ^{44}Ca enrichment, Oak Ridge National Laboratory, Oak Ridge, TN) in 154 mM NaCl, pH 7.2, was injected into the duodenal lumen of the ether-anesthetized chickens, and absorption proceeded for 2.5, 5.0, and 20.0 min. At the end of the absorption period, the lumen of each segment was thoroughly rinsed *in situ* with 154 mM NaCl, and the mucosa was exposed with blood supply still intact. A small flap of intestine was immediately frozen by the cryo-press technique (7), by using liquid N_2-cooled copper pliers. Two-micrometer-thick cryosections of the frozen tissue were obtained by using Reichert's Cryo-Cut II microtome in the -30 to -25°C range. The frozen sections were mounted on a liquid nitrogen-cooled indium substrate and freeze-dried before ion microscopic analysis (8).

A Cameca IMS-3f ion microscope (Cameca, Paris), operating with an 8-keV O_2^+ primary ion beam, was used in this study to monitor positive secondary ions. For isotopic images in Fig. 2, a mass-filtered 400-nA O_2^+ primary-ion beam (spot size of ≈ 60 μm) was directed onto a 500-μm-square raster. The secondary ions were extracted from a circular region (400 μm in diameter) centered within the raster. For isotopic images in Fig. 3 *Left* and *Right*, a 250-nA O_2^+ primary-ion beam (spot size of ≈ 60 μm) was directed onto a 250-μm-square raster. A 60-μm contrast aperture was used in the imaging mode throughout the study. High-resolution mass

The publication costs of this article were defrayed in part by page charge payment. This article must therefore be hereby marked "*advertisement*" in accordance with 18 U.S.C. §1734 solely to indicate this fact.

Abbreviation: CCD, charge-coupled device.

scans ($m/\Delta m \approx 5000$) were performed to check for mass-interference components in the secondary-ion signals from $^{44}Ca^+$, $^{40}Ca^+$, $^{39}K^+$, $^{23}Na^+$, and $^{12}C^+$. A 750-μm field aperture was used in the spectrometer for high-mass-resolution analyses. Tissue cryosections after 20 min of ^{44}Ca absorption from vitamin D-deficient and vitamin D-replete treatments were used for high-mass-resolution analyses because uninjected controls revealed barely detectable $^{44}Ca^+$ secondary-ion signals. None of studied secondary-ion signals suffered from any significant mass interferences. The purity of $^{44}Ca^+$ and $^{40}Ca^+$ signals was ≈98% ($n = 4$). Over 99% purity was seen for $^{39}K^+$, $^{23}Na^+$, and $^{12}C^+$ signals. These observations imply that low-mass-resolution imaging clearly reveals spatial distributions of masses 44, 40, 39, 23, and 12 without any significant mass interferences in this tissue. Significant mass interferences previously noted for ^{44}Ca stable calcium are possibly due to the use of silicon substrate under the O_2^+ beam, which is conducive to the formation of the $^{44}(SiO^+)$ species, as well as the plastic embedment used in that study (9).

The secondary ion images of isotopes with masses of 44, 40, 39, 23, and 12 revealed the tissue localization of $^{44}Ca^+$, $^{40}Ca^+$, $^{39}K^+$, $^{23}Na^+$, and $^{12}C^+$, respectively, and these images were acquired for digital processing, using a charge-coupled device (CCD) imager (Photometrics, Tucson, AZ, model CH220 CCD liquid-cooled camera head equipped with a Thomson-CSF TH7882 CDA CCD). The CCD was operated in a 2 × 2 binning mode, and the CCD output was digitized to 14 bits per pixel by a Photometrics camera controller. The details of the high sensitivity and extremely linear response of the CCD imager have been documented (10). The image processing was done by using a PDP 11/34-based system and a secondary ion-mass-image processing program (11). The final processed images were recorded on Kodak T Max (ASA 100) film from the display monitor and printed for optimal image quality.

The overall absorption and tissue retention of calcium were quantitated in comparable chickens by the use of the radionuclide ^{47}Ca and essentially by the same absorption technique as described above. In these experiments, the intraluminal dosing solution contained 20 mM ^{40}Ca as the chloride in 154 mM NaCl, pH 7.2, and 0.1 μCi of ^{47}Ca (1 Ci = 37 GBq). After absorption periods of 2.5, 5.0, and 20.0 min, the duodenal segment was removed *in toto*, placed in a counting

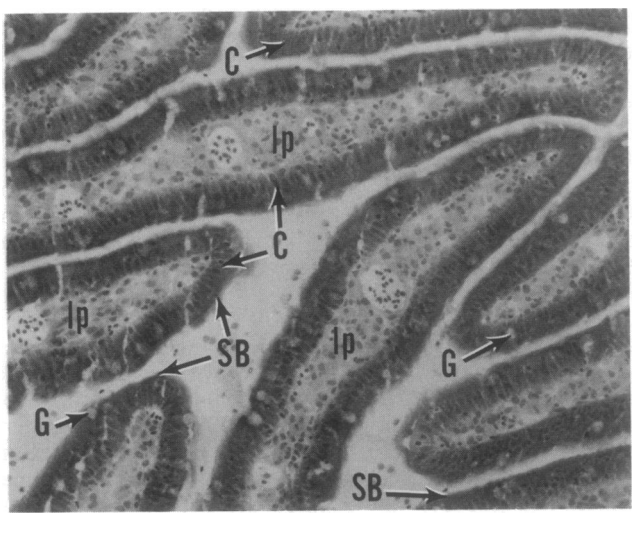

FIG. 1. A light micrograph showing morphological preservation in a cryosection from vitamin D-deficient treatment after 20 min of ^{44}Ca absorption. The surface epithelium shows goblet cells (G) and columnar cells (C) with striated border (SB). The lamina propria (lp) contains blood and lymph vessels. (×150.)

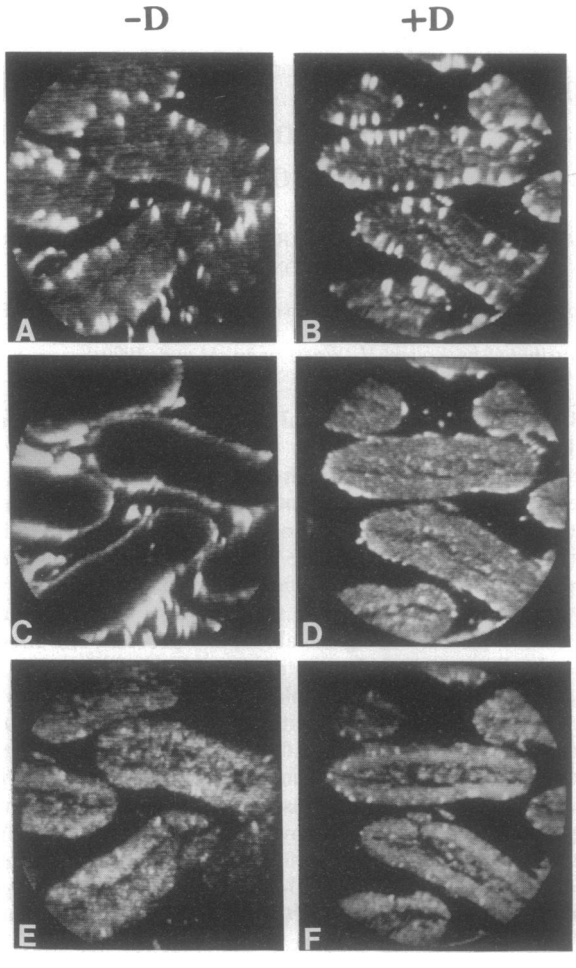

FIG. 2. Secondary ion images of $^{40}Ca^+$, $^{44}Ca^+$, and $^{39}K^+$ representing intravillus distribution of isotopes 40, 44, and 39, respectively, in vitamin D-deficient (−D) and vitamin D-replete (+D) chickens after 20 min of intraluminal ^{44}Ca administration. Within each treatment, a few longitudinally sectioned villi are seen with their isotopic distributions. (*A* and *B*) Secondary ion images of $^{40}Ca^+$ (naturally occurring calcium). (*C* and *D*) Secondary ion images of $^{44}Ca^+$ (transported calcium). (*E* and *F*) Secondary ion images of $^{39}K^+$, tissue potassium. Mass-40 and -44 images were integrated for 150 sec directly on the CCD camera from the microchannel plate-fluorescent screen assembly of the ion microscope. Similarly, mass-39 images were recorded for 0.4 sec. The CCD output was digitized to 14 bits (16,384 grey levels) and corrected for dark current. The raw image thus formed was scaled down (divided) by a factor to display the raw image between 0 to 255 grey levels. The scale-down factor was decided by processing the individual images for their image quality alone. In the vitamin D-replete case, scale-down factors for the individual raw images were as follows: mass 40 = 30; mass 44 = 12; and mass 39 = 17. In the vitamin D-deficient treatment, scale-down factors for the individual raw images were as follows: mass 40 = 25; mass 44 = 25; and mass 39 = 14. In both treatments, $^{40}Ca^+$ intensities from goblet cells are shown saturated, so that other areas can be visualized. The natural abundance of ^{44}Ca is 2.09%. This contribution was corrected from the mass-44 image by digitally registering (overlaying) and subtracting the 2.09% fraction of a corrected mass-40 image from the mass-44 image. The isotopic composition of the injected stable ^{44}Ca was as follows: 44 = 98.78%, 40 = 1.12%, 42, 43, 46, and 48 = <0.06% each. Therefore, the 1.12% contribution from the mass-40 image was corrected in a similar way as described above. Because of very high enrichment of stable ^{44}Ca and low natural abundance of this isotope, these corrections were minor and made no significant change in the image. The tissue sections from both treatments showed higher signals for potassium than sodium. The $^{12}C^+$ ion images, representing carbon distribution, were homogenous throughout the tissue. The carbon and sodium ion images are not shown here. (Diameter of the circular region of the images is 400 μm.)

vial with ice-cold saline, and counted for radioactivity for 1 min in a γ scintillation counter (Beckman model γ 300). The difference between those counts and amount of ^{47}Ca injected yielded the value of ^{47}Ca absorbed. The segment was then drained, and the lumen was rinsed with 20 ml of cold saline to remove unabsorbed luminal ^{47}Ca; the radioactivity of the segment was then recounted, yielding the amount of ^{47}Ca retained by the tissue. Data are expressed as percentage of the administered dose.

RESULTS

Fig. 1 is a light micrograph of a cryosection from the duodenum stained with hematoxylin/eosin. The tissue was from a vitamin D-deficient chicken obtained after the 20-min absorption period and depicts the usual gross morphological features of this tissue. Longitudinally oriented villi are shown. Discernable are goblet cells (G), columnar epithelial cells (C), the striated border (SB), and the lamina propria (lp), the latter containing blood and lymph vessels. This figure, in addition to demonstrating morphological preservation of the tissue during processing, also provides orientation for the following ion microscopic images.

Fig. 2 depicts ion microscopic images comparing intestinal localization of transported calcium (mass 44), the major isotope of naturally occurring calcium (mass 40, ≈97% abundance), and the major isotope of potassium (mass 39, ≈93% abundance) between the vitamin D-deficient and vitamin D-replete chickens after 20 min of intraluminal ^{44}Ca administration. Several villi, sectioned longitudinally, are shown with their isotopic distributions. Brightness indicates relative isotopic intensity within an image. The naturally occurring calcium is heterogeneously distributed throughout the villus with the goblet cells showing a very high accumulation in both treatments (*A* and *B*). The transported calcium (mass 44), however, shows a remarkable difference in localization due to vitamin D repletion (*C* and *D*). In the section from the vitamin D-deficient chickens, ^{44}Ca is concentrated in the microvillar/terminal web region of the epithelial cell; little ^{44}Ca is evident beneath this region or in the lamina propria. In contrast, ^{44}Ca is more diffusively distributed in the vitamin D-replete tissue, present throughout the enterocyte and in the lamina propria. Note that the goblet cells, which sequester high concentrations of ^{40}Ca, are not "labeled" with ^{44}Ca, indicating that goblet cell calcium does not exchange or only at a slow rate. Potassium is well distributed within the enterocytes and the lamina propria (*E* and *F*). Some goblet cells appear to contain relatively large amounts of K^+. These

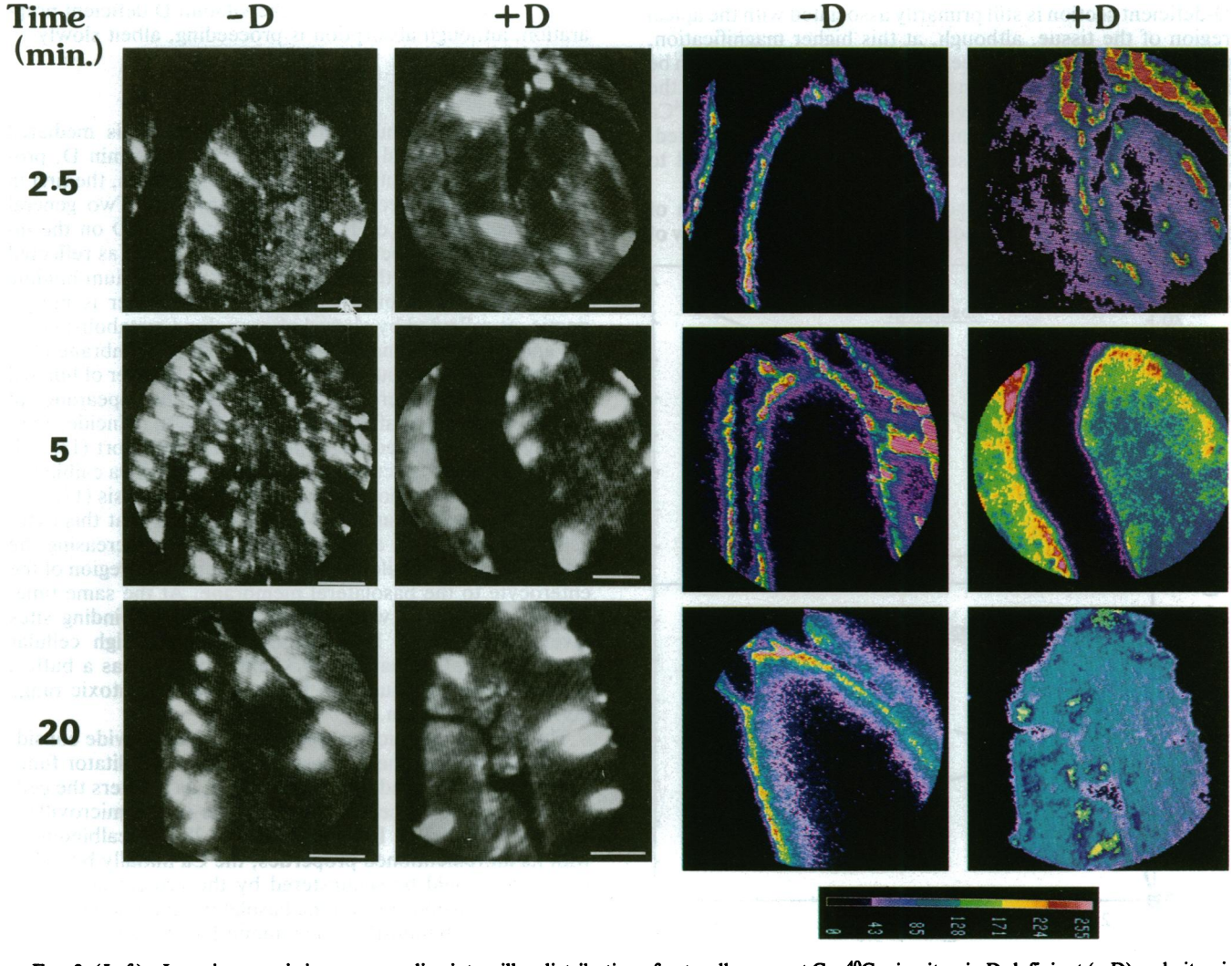

FIG. 3. (*Left*) Ion microscopic images revealing intravillus distribution of naturally present Ca, ^{40}Ca, in vitamin D-deficient (−D) and vitamin D-replete (+D) chickens at 2.5, 5.0, and 20.0 min of absorption. Ion images were corrected for isotopic abundances, as described in Fig. 2 legend. Each image contains portions of at least one longitudinally sectioned villus. Individual $^{40}Ca^+$ images were processed for optimal image quality. The goblet cells are shown saturated. (Bars = 20 μm.) (*Right*) Respective transported $^{44}Ca^+$ images from these same tissues after the same periods of absorption. The individual $^{44}Ca^+$ image was processed for optimal image quality. Magnification is comparable between *Left* and *Right*. Color scale shows pixel intensities from 0 to 255.

observations were repeated twice, and >20 longitudinally sectioned villi were recorded for these observations.

Fig. 3 *Left* and *Right* depicts the ion microscopic images of ^{40}Ca and ^{44}Ca, respectively, in cryosections of duodena taken at the different periods of absorption and at a higher magnification than in Fig. 2. The ion images of transported ^{44}Ca, shown in Fig. 3 *Right*, are in pseudocolor.

The naturally occurring calcium ^{40}Ca distribution, once again, shows no apparent difference in its intestinal localization between vitamin D-deficient (−D) and vitamin D-replete (+D) chickens (Fig. 3 *Left*). Location of goblet cells is evident by their intensity.

The localization of transported calcium (^{44}Ca) as a function of time and treatment is presented in Fig. 3 *Right*. At 2.5 min of absorption, ^{44}Ca is concentrated in the brush border region in both vitamin D-deficient and -replete chickens, although some transmural movement of ^{44}Ca is seen in vitamin D-replete duodenum. At 5.0 min, the distribution pattern in the vitamin D-deficient duodenum is about the same as at 2.5 min, but a distinct change in the localization of ^{44}Ca in the vitamin D-replete duodenum can be seen. For the latter, there is a diminishing difference between the intensities of ^{44}Ca localized in the brush border region and in the remainder of the enterocyte and in the lamina propria. At 20 min, and as shown before in Fig. 2 *C* and *D*, ^{44}Ca in the vitamin D-deficient section is still primarily associated with the apical region of the tissue, although, at this higher magnification, the concentration of ^{44}Ca deeper within the enterocyte can be seen to have increased considerably as compared with the earlier time periods. In the vitamin D-replete tissue, the ^{44}Ca remaining in the tissue is almost homogeneously distributed. At least 10 longitudinally sectioned villi were recorded to confirm these observations.

Determination of the absorption and tissue retention of radioactive ^{47}Ca provides a quantitative and dynamic view of

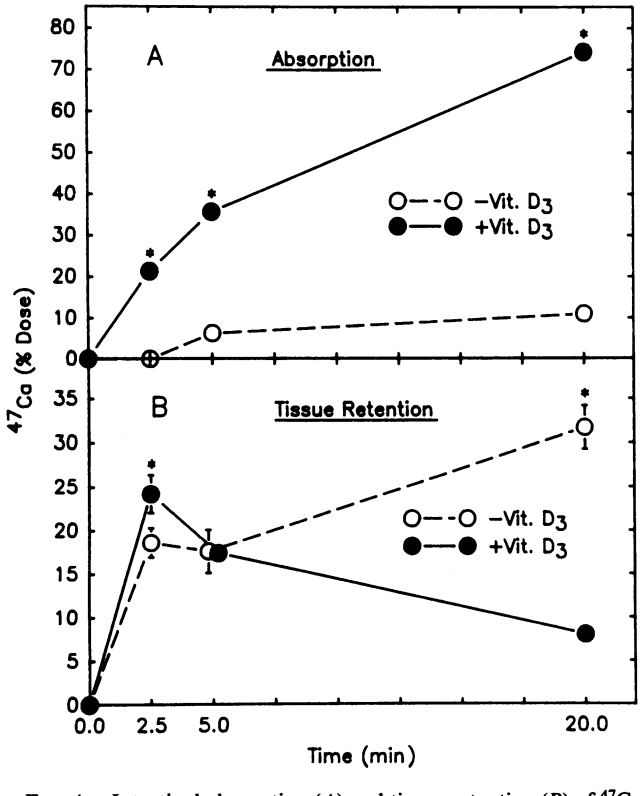

FIG. 4. Intestinal absorption (*A*) and tissue retention (*B*) of ^{47}Ca (20 mM $^{40}CaCl_2$) injected into the lumen of vitamin D-deficient (−Vit. D_3) and replete (+Vit. D_3) chickens for the periods indicated. *, Significant difference ($P > .05$) between +Vit. D_3 and −Vit. D_3 values.

events during the same time periods that were used in the ion microscopic study. The expected stimulatory effect of vitamin D on ^{47}Ca absorption is shown in Fig. 4*A*, where significant differences exist at all time points. At 20 min ≈74% of the intraluminal Ca was absorbed by the vitamin D-replete chickens, and only ≈11% by the vitamin D-deficient chickens. The tissue retention data are, perhaps, more meaningful in terms of the primary objective of this study. At 2.5 min, the vitamin D-replete tissue content of ^{47}Ca was significantly greater than that of the vitamin D-deficient tissue, indicative of a more rapid transfer of luminal Ca across the brush border membrane due to vitamin D. Thereafter, the tissue level of ^{47}Ca in the vitamin D-replete chickens decreased, reflecting both the extrusion of Ca from the epithelium in the direction of the lamina propria and a decrease in ^{47}Ca in the precursor luminal compartment from the overall absorption process. In contrast, the intestinal tissue level of ^{47}Ca of the vitamin D-deficient chickens steadily increased with time, reflecting the less rapid extrusion of Ca from the tissue. These kinetic data are consistent with the ^{44}Ca ion microscopic images (Figs. 2 and 3), the latter clearly showing that absorbed Ca in the vitamin D-replete cryosections initially (at 2.5 min) accumulates in the region subjacent to the microvillar membrane and moves away from this region later. In contrast, ^{44}Ca remains highly concentrated in the brush border/terminal web region of the vitamin D-deficient preparation, although absorption is proceeding, albeit slowly.

DISCUSSION

The vitamin D stimulation of Ca absorption is mediated through its hormonal form, 1,25-dihydroxyvitamin D, produced by two sequential hydroxylation reactions, the first in the liver and the second in the kidney (12). Two general biochemical actions of 1,25-dihydroxyvitamin D on the intestine have been documented. One is genomic, as reflected by the synthesis of the vitamin D-induced calcium-binding protein, 28-kDa calbindin-D (13), and the other is nongenomic, as reflected by altered phospholipid metabolism (13–15) and increased fluidity of the microvillar membrane (16). The latter might account for the increased transfer of luminal calcium into the enterocyte (cf. Fig. 4*B*). The appearance of 28-kDa calbindin-D after vitamin D repletion coincides temporally with enhanced transepithelial Ca transport (13). Although the exact function (or functions) of 28-kDa calbindin-D in this process is not known, theoretical analysis (17) with some experimental support (18, 19) suggests that this cytosolic protein acts as a diffusional facilitator, increasing the rate of diffusion of calcium from the microvillar region of the enterocyte to the basolateral membrane. At the same time, 28-kDa calbindin-D with its four half-affinity binding sites (average $K_d \approx 5 \times 10^{-7}$ M) and relatively high cellular concentration (estimated at 0.3 mM) could act as a buffer, maintaining intracellular Ca levels within a nontoxic range during Ca absorption.

The present ion microscopic imaging data provide considerable support for the proposed diffusional facilitator function of 28-kDa calbindin-D. Luminal Ca, as it enters the cell, appears to bind to cellular components in the microvillar/terminal web region. In the presence of 28-kDa calbindin-D, with its aforementioned properties, the Ca initially bound to this region could be sequestered by the protein and transferred to extrusion sites on the basolateral membrane. Without 28-kDa calbindin-D in the vitamin D-deficient tissue, Ca in transit remains highly concentrated in the brush border region and only slowly diffuses away from this region, accounting for the diminished rate of absorption. An earlier study based on ^{45}Ca autoradiographic, microincineration, and electron microscopic methodology similarly indicated that, in the rachitic rat, absorbed Ca binds to components in

the microvillar region and that vitamin D in some fashion mobilizes Ca from this region (22).

Another proposed mechanism of intracellular transport is by way of an endocytotic–exocytotic–vesicular flow process (20). Luminal Ca, sequestered in endocytotic vesicles at the brush border membrane, is thought to move through the cell interior in membrane-encapsulated forms and to be released into the lamina propria by exocytosis. The 28-kDa calbindin-D was considered to have a role in the vesicular flow process because this protein was reported to associate with microtubules and, in addition, a small percentage of total cellular 28-kDa calbindin-D was localized in vesicles and lysosomes (20). Although neither the diffusional facilitator model nor the vesicular flow models have been proven, both models implicate the 28-kDa calbindin-D in the absorptive process, and each could theoretically account for the ion microscopic images reported herein.

Further, it should be considered that the binding of Ca to components of the brush border region might have a homeostatic regulatory function in terms of controlling ionized Ca concentrations within the enterocyte. As a possibility, binding of Ca within this region might exert an inhibitory effect on the further entrance of Ca into the cell by altering the Ca permeability of the lipid membrane. In this way, the unhindered entrance of luminal Ca down its steep electropotential gradient into the cell could be controlled, protecting the cell from the toxic effects of this element. The nature of the Ca-binding components subjacent to the microvillar membrane is not known, but cytoskeletal elements and Ca-binding proteins, including calmodulin (21), are likely candidates.

This study, in addition to providing additional information on the Ca absorptive process and the intestinal effects of vitamin D, illustrates the investigative advantage of the use of ion microscopy in combination with stable isotope tracers to visualize the cellular features associated with the transport of ions and, perhaps, other substrates across epithelia.

This work was supported by National Institutes of Health Grants GM24314, ES04072, and DK04652.

1. Rasmussen, H. & Waisman, D. M. (1983) *Rev. Physiol. Biochem. Pharmacol.* **95,** 111–148.
2. Casting, R. & Slodzian, G. (1962) *J. Microsc. (Paris)* **1,** 395–410.
3. Morrison, G. H. & Slodzian, G. (1975) *Anal. Chem.* **47,** 932A–943A.
4. Chandra, S. & Morrison, G. H. (1988) *Methods Enzymol.* **158,** 157–179.
5. Edelstein, S., Fullmer, C. S. & Wasserman, R. H. (1984) *J. Nutr.* **114,** 692–700.
6. Morrissey, R. L. & Wasserman, R. H. (1971) *Am. J. Physiol.* **220,** 1509–1515.
7. Hagler, H. K., Lopez, L. E., Flores, J. S., Lundswick, R. S. & Buja, L. M. (1983) *J. Microsc. (Oxford)* **131,** 221–234.
8. Sod, E. W., Morrison, G. H. & Crooker, A. (1990) *J. Microsc. (Oxford)*, in press.
9. Burns, M. S. (1984) *J. Microsc. (Oxford)* **135,** 209–212.
10. Mantus, D. S. & Morrison, G. H. (1990) *Anal. Chem.* **62,** 1148–1155.
11. Ling, Y.-C., Bernius, M. T. & Morrison, G. H. (1987) *J. Chem. Inf. Comput. Sci.* **24,** 86–95.
12. DeLuca, H. F. (1984) in *Vitamin D-Basic and Clinical Aspects*, ed. Kumar, R. (Nijhoff, Boston), pp. 1–68.
13. Wasserman, R. H., Brindak, M. E., Meyer, S. A. & Fullmer, C. S. (1982) *Proc. Natl. Acad. Sci. USA* **79,** 7939–7943.
14. O'Doherty, P. J. A. (1979) *Lipids* **14,** 75–77.
15. Matsumoto, T., Fontaine, O. & Rasmussen, H. (1981) *J. Biol. Chem.* **256,** 3354–3360.
16. Brasitus, T. A., Dudeja, P. K., Eby, B. & Lau, K. (1986) *J. Biol. Chem.* **261,** 16404–16409.
17. Kretsinger, R. H., Mann, J. E. & Simmonds, G. G. (1982) in *Vitamin D: Chemical, Biochemical and Clinical Endocrinology of Calcium Metabolism*, eds. Norman, A. W., Schaefer, K., Herrath, D. V. & Grigoleit, H.-G. (de Gruyter, New York), pp. 233–248.
18. Feher, J. J. (1983) *Am. J. Physiol.* **244,** C303–C307.
19. Feher, J. J., Fullmer, C. S. & Fritzsch, G. K. (1989) *Cell Calcium* **10,** 189–203.
20. Nemere, I., Leathers, V. L. & Norman, A. W. (1986) *J. Biol. Chem.* **261,** 16106–16114.
21. Bikle, D. D., Munson, S. & Chafouleas, J. G. (1984) *Prog. Clin. Biol. Res.* **168,** 193–197.
22. Sampson, H. W., Matthews, J. L., Martin, J. H. & Kunin, A. S. (1970) *Calcif. Tissue Res.* **5,** 305–316.